Analysing Events With Z Bosons With The Atlas Experiment

Third Year Lab Report

James Parker: 10694426
Department of Physics and Astronomy, University of Manchester
(Experiment performed in collaboration with R. Soares)
(Dated: April 23, 2024)

This report presents the findings from the analysis of Z boson production and decay in proton-proton collisions at the Large Hadron Collider, using the ATLAS 13 TeV open data set. The objective was to measure the cross sections for $Z \to e^- + e^+$ and $Z \to \mu^- + \mu^+$ decays and compare with predictions from the Standard Model. Data were selected and analysed using selection criteria optimised to isolate Z boson decay events and reduce background noise. Monte Carlo simulations, along with a data-driven method for background correction, were used to estimate and correct for remaining background contributions not filtered by the selection criteria. The measured cross sections, $\sigma(pp \to Z \to \mu^- + \mu^+) = 1.967 \pm 0.001(stat.) \pm 0.025(syst.) \pm 0.033(lumi.)$nb and $\sigma(pp \to Z \to e^- + e^+) = 2.004 \pm 0.001(stat.) \pm 0.024(syst.) \pm 0.034(lumi.)$nb, are in excellent agreement with the Standard Model and similar experiments.

1. INTRODUCTION

The Standard Model (SM) is recognised as the most accurate framework in particle physics. It categorises all known particles as either fermions or bosons. The Z boson, as well as the $W^{+/-}$ bosons are responsible for mediating the weak nuclear force. The Z boson was predicted by the electroweak unification theory, a fundamental aspect of the SM proposed by Glashow, Salam and Weinberg in 1967 [1]. It posits that the electromagnetic and weak nuclear forces can be described by a single theoretical framework at high energies. Within this framework, the Z boson facilitates the transmission of the weak force without altering the electric charge of the involved particles.

The principle of Lepton universality in the SM asserts that gauge bosons couple with equal strength to all three flavours of leptons, suggesting that the Z boson should have an identical cross section for decaying into any lepton-antilepton pair. With a mass of $91.188 \pm 0.002 GeV/c^2$ [2], the Z boson is significantly heavier than any of the leptons, ensuring that decays into lighter leptons are not kinematically favoured, a prediction confirmed by this experiment.

Our study utilises data from the ATLAS detector at the Large Hadron Collider (LHC) in CERN, which detects the final products of proton-proton collisions. The 2016 open data from the ATLAS experiment, which recorded collisions at a centre-of-mass energy of $\sqrt{s} = 13$ TeV, combined with Monte Carlo (MC) simulations, provided insights into the processes of Z boson decays into e^-e^+ and $\mu^-\mu^+$ pairs. Using selection cuts on the experimental data, we enhance the signal-noise ratio enabling precise measurements of the cross sections for each decay channel.

2. THEORY

2.1. Electroweak Unification Theory

The Electroweak Unification Theory extends quantum electrodynamics by including the weak force. It predicts that the electromagnetic (EM) and weak force merge into a single electroweak force at high energy levels, facilitated by the Higgs field [3]. At lower energies, symmetry breaking differentiates the two forces, crucial for explaining the infinite range of the EM force compared to the weak force's range of approximately 0.1 fm. The symmetry breaking, enabled by the Higgs mechanism, provides mass to the W and Z bosons, unlike the photon, which remains massless due to it non-interaction with the Higgs field.

2.2. Production of Z Bosons at the LHC

The LHC at CERN is the most powerful particle accelerator in operation, facilitating high-energy proton-proton collisions. Protons, comprising of quarks bound by gluons, exhibit complex internal dynamics. According to the energy-time uncertainty principle,

$$\Delta E \cdot \Delta t \geq \frac{\hbar}{2}, \tag{1}$$

a sea of gluon-induced quark-antiquark pairs surrounds the valence quarks. At high energies, these quarks and antiquarks behave as nearly free particles, leading to Z boson production upon their collision [3].

2.3. Decay Channels and Lepton Universality

The Z boson can decay into any fermion-antifermion pair, except for $t\bar{t}$ as the the mass of the top quark ($172.69 \pm 0.3 GeV/c^2$) exceeds half of the Z bosons mass [4]. Despite the mass dependency of decay rates, the Z boson's considerable mass relative to any lepton allows it to decay into any lepton pair without kinematic restrictions. The near identical observed branching ratios, approximately 3.4% [2], confirm the principle of lepton universality which asserts equal gauge boson coupling constants across all lepton families.

2.4. Event Selection

For the analysis of Z boson decay into e^-e^+ and $\mu^-\mu^+$, the selection criteria focuses on the invariant mass distribution, particle isolation and detector acceptance. The invariant mass of the decay products is given by,

$$m_{ll} = \sqrt{2 p_{T1} p_{T2} \left(\cosh(\eta_1 - \eta_2) - \cos(\phi_1 - \phi_2)\right)}, \tag{2}$$

where $p_{T1/T2}$ represent the transverse momenta, $\eta_{1/2}$ denote the pseudorapidities and $\phi_{1/2}$ refer to the azimuthal angles between the interaction point and the beam axis for each of the two decay particles. As depicted in Figure 1, the Z boson mass peak is easily distinguishable amongst background processes and is a useful tool when trying to isolate signal events due to its conservation in all reference frames [5].

Particle isolation comes from the need to distinguish signal events from background processes originating from jets. Jets are sprays of hadrons produced from the hadronisation of gluons from the initial proton-proton collision. These processes can mimic the leptonic decays of Z bosons. Two variables that can help suppress these backgrounds are E_T^{cone} and P_T^{cone} which respectively measure the sum of the transverse energy and momentum within a defined cone around the direction of the lepton. Events that arise from Z boson decays are expected to be isolate, not accompanied by significant transverse energy and momentum that would be expected with jets.

To distinguish between signal events and background events originating from jets, we can enforce particle isolation. Jets are sprays of hadrons produced from the hadronisation of gluons from the initial proton-proton collision which can mimic the leptonic decays of Z bosons. Events that arise from Z boson decays are expected to be isolated, not accompanied by significant transverse energy

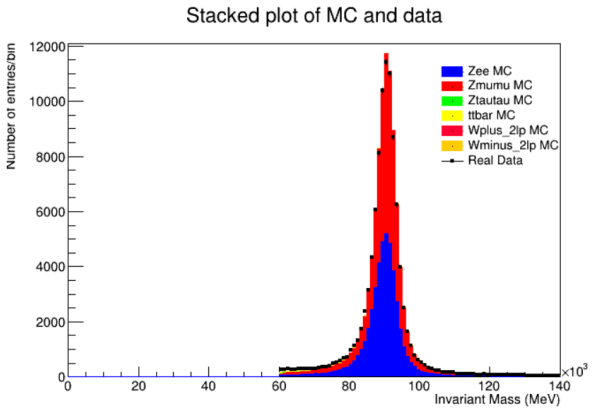

FIG. 1. Histogram of invariant mass distribution for events with two leptons of the same flavour and opposite charge

and momentum that would be expected with jets. E_T^{cone} and P_T^{cone} respectively measure the sum of the transverse energy and momentum within a defined cone around the direction of the lepton.

The barrel region of the detector surrounds the collision point and measures trajectories and energies of particles produced in collisions with higher resolution. This region can be targeted using pseudorapidity, given by $\eta = -ln\left[\tan\left(\frac{\theta}{2}\right)\right]$ where θ is the polar angle between the detection point and the beam axis. Events occurring closer to the collision point, and therefore measured with greater accuracy, have a lower magnitude of η.

2.5. *Cross sections*

Cross sections quantify the likelihood of an interaction occurring between particles in a collision. In this experiment the cross sections were calculated with,

$$\sigma = \frac{N^{selected} - N^{background}}{\epsilon \int L\,dt}, \tag{3}$$

where $N^{selected}$ denotes events passing the selection criteria, $N^{background}$ represents the estimated background events, ϵ is signal event selection efficiency, and $\int L\,dt$ is the integrated luminosity, given as $10.064 fb^{-}1$ [6]. ϵ is the fraction of signal MC events passing the selection criteria:

$$\epsilon = N_{pass}^{signal} / N_{total}^{signal}. \tag{4}$$

3. EXPERIMENTAL APPROACH

3.1. *Choosing selection cuts*

We began by establishing basic criteria that would preserve all potential signal event, requiring an event must contain only two leptons of opposite charge and the same flavour (electron or muon dependent on the cross section measurement). Additionally, a minimum invariant mass cut was implemented at 60 GeV due to the Monte Carlo data only containing events exceeding this value. Our three targeted areas outlines in section 2.4 brought us to optimise six variables: minimum and maximum invariant mass, minimum and maximum pseudorapidity, and maximum values for E_T^{cone} and P_T^{cone}. The criteria for optimising these variables was to maximise significance,

$$Significance = \frac{N^{signal}}{\sqrt{N^{background}}}. \tag{5}$$

Using $\sqrt{N^{background}}$ helps to prevent disproportionate weighting of cut values that only remove a small number of background events due to there being far few background events compared to signal events.

The optimisation process involved two phases. Initially, we set cuts that would not exclude any signal events as a baseline, referenced above. Each of the six variables was then varied individually across a large range, to a resolution of two significant figures around the optimum value.

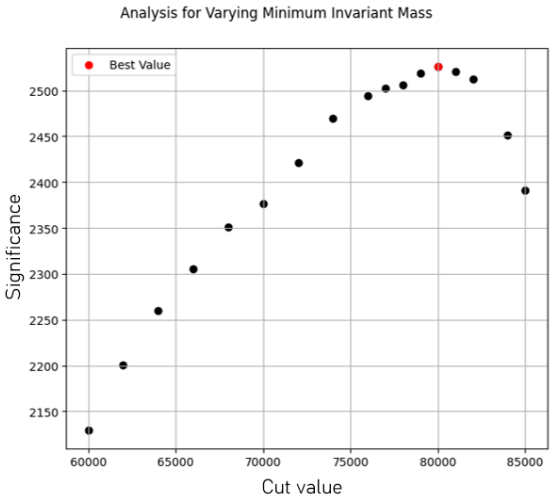

FIG. 2. Plot of $SignificancevsCutvalue$ for the minimum invariant mass selection cut, with the optimum value indicated.

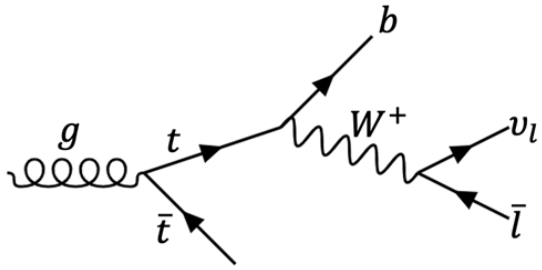

FIG. 3. Feynman diagram of a gluon decaying to a $t\bar{t}$ pair, which decay to two leptons and two neutrinos.

An example of this optimisation for minimum invariant mass is given in Figure 2. This iterative process of individual variable optimisation was repeated for each variable. The optimal values then established the baseline for the next phase which we called 'Base cut 2', where the entire process was repeated to determine our final selection cuts.

3.2. *Background Signal*

By applying the same selection cuts to both the ATLAS and MC data, the number of MC background events that pass can be used as an estimate for the corresponding number of background events in the ATLAS data, $N^{background}$.

However, not all background events are captured by the Monte Carlo simulations, an example is depicted in Figure 3. Such processes lead to the same final product products as our signal via different decay pathways. While our Z boson decays specifically into two leptons of the same flavour, these processes could decay into two leptons of any flavour, reflecting lepton universality. To estimate the number of background e^+e^- and $\mu^+\mu^-$ events, we count the number of $e\mu$ events that passed the selection cuts (barring the requirement that both leptons must be the same flavour). We then created a correction factor for $N^{background}$, given by,

$$CorrectionFactor = \frac{N_{e\mu}^{selected}}{N_{e\mu}^{signal} + N_{e\mu}^{background}}. \tag{6}$$

This helps to prevent counting a single background event twice, once in the MC and once again from this estimate, by using the excess of $e\mu$ events in the ATLAS data compared to the prediction from the MC data.

4. RESULTS

4.1. Errors

For our cross section measurements we had three types of errors: statistical, systematic and a luminosity error. The fractional uncertainty on the integrated luminosity is given in documentation as 1.7% [6].

The statistical uncertainty in our measurements stems from a Poisson counting error. The number of events, N, follows a Poisson distribution due to the random nature of particle interactions. The standard deviation is given by,

$$\Delta N = \sqrt{N}. \tag{7}$$

The total statistical uncertainty, considering we have a measurement of $N^{selected} - N^{background}$, must consider,

$$\Delta N^{total} = \sqrt{\Delta N^2_{\text{selected}} + \Delta N^2_{\text{background}}}, \tag{8}$$

along with the fractional uncertainty on ϵ, and is given by,

$$\Delta\sigma^2 = \sigma^2 \sqrt{\left(\frac{\Delta\epsilon}{\epsilon}\right)^2 + \left(\frac{\Delta N^{total}}{N^{total}}\right)^2}. \tag{9}$$

To estimate the systematic uncertainty, we analysed the variation in our measured cross sections before and after optimising an individual selection cut. For each variable, the systematic uncertainty is the difference between the cross section calculated using the standard set of cuts, 'Base cut 2' (shown in Table I), and the cross section when 'Base cut 2' was compounded with the additionally optimised variable. These discrepancies originate from distinct aspects of variable optimisation so are considered independent. They are summed in quadrature to obtain the total systematic uncertainty.

4.2. Cross section measurements

The measured cross sections were measured to be:
$\sigma_{\mu^-\mu^+}$=1.967±0.001(stat)±0.025(syst)±0.033(lumi) nb
$\sigma_{e^-e^+}$=2.004±0.001(stat)±0.024(syst)±0.034(lumi) nb
These measurements were achieved with the Final Cuts, detailed in Table I.

Cut	Base Cuts 2		Final Cuts	
	$Z \to e^+e^-$	$Z \to \mu^+\mu^-$	$Z \to e^+e^-$	$Z \to \mu^+\mu^-$
Max m_{ll}	108 GeV	103 GeV	96 GeV	95 GeV
Min m_{ll}	80 GeV	82 GeV	82 GeV	86 GeV
Max E_T^{cone}	5200 MeV	5500 MeV	3100 MeV	2100 MeV
Max P_T^{cone}	4100 MeV	5000 MeV	2000 MeV	3100 MeV
Min η	-2.5	-2.7	-2.7	-2.9
Max η	2.5	2.8	3.3	2.9
Cross-section	2.013 nb	1.980 nb	2.004 nb	1.967 nb
Significance	37312	48305	45471	59777

TABLE I. Selection cuts and Cross section measurements for two optimisation stages, showing an increase in significance.

5. DISCUSSION AND CONCLUSION

Electrons, as they pass through the detector material, are significantly affected by bremsstrahlung radiation compared to muons due to their lower mass and therefore greater deflection by the magnetic field. Consequently, we have looser cuts on E_T^{cone} and minimum m_{ll} for electrons relative to muons. The electrons lose energy when they are detected so have a lower measured invariant mass and are accompanied by energy around their interaction point. To balance the greater background retention from looser E_T^{cone} cuts, a tighter P_T^{cone} cut is applied, relative to muons, to effectively remove jets.

The observed discrepancy on the left side of the Z peak in Figure 4 suggests the MC simulations underestimate the effects of bremsstrahlung on electron signal events, leading to an inadequate representation of the low-mass tail. Despite this, our cross section measurements align within error margins and are consistent with the Standard Model's prediction of identical electroweak interactions between these pairs. This agreement supports the Standard Model, although the noted simulation discrepancy suggests areas for improvement in our computational models.

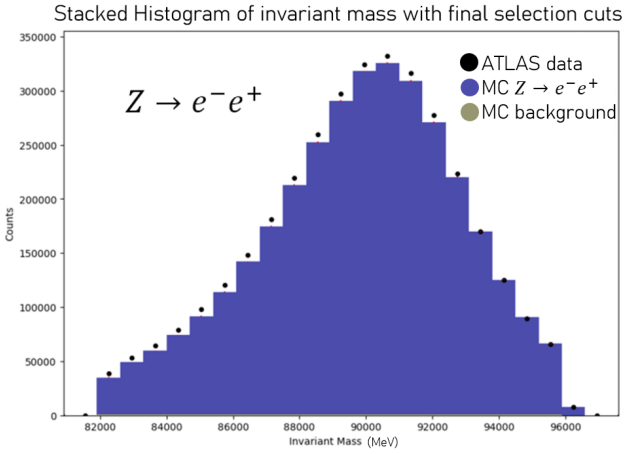

FIG. 4. Stacked Histogram of invariant mass distribution for $Z \to e^+e^-$ events, with final cuts applied

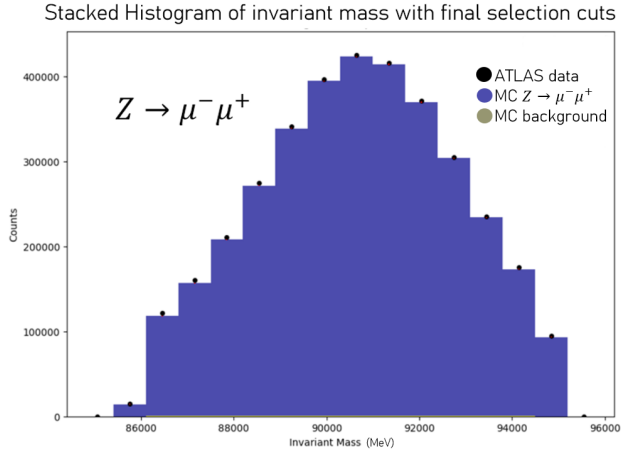

FIG. 5. Stacked Histogram of invariant mass distribution for $Z \to \mu^+\mu^-$ events, with final cuts applied

[1] J.-F. Gauvin, En route to a grand unified theory: The unification of electromagnetism and the weak nuclear force at the turn of the 1970s, Encyclopedia.com (2024), available from: https://www.encyclopedia.com, Accessed: April 22, 2024.

[2] M. Tanabashi *et al.*, Physical Review D **98**, 030001 (2018).

[3] B. R. Martin and G. P. Shaw, *Particle Physics* (Wiley, Chichester, 2008) available from: ProQuest Ebook Central. [Accessed: 22 April 2024].

[4] R. L. Workman *et al.*, Prog. Theor. Exp. Phys. **2022**, 083C01 (2022).

[5] Wikipedia contributors, Invariant mass — Wikipedia, the free encyclopedia, https://en.wikipedia.org/wiki/Invariant_mass (2024), [Online; accessed 22-April-2024].

[6] ATLAS Collaboration, *Luminosity determination in pp collisions at* $\sqrt{s} = 13$ *TeV using the ATLAS detector at the LHC*, ATLAS Conference Note ATLAS-CONF-2019-021 (CERN, Geneva, 2019) available at https://cds.cern.ch/record/2677054.